Control of nitrogen atomic density and enthalpy flow into reaction chamber in Ar/N2 pulse-modulated induction thermal plasmas

著者	Tanaka Yasunori, Muroya Takafumi, Hayashi Kohei, Uesugi Yoshihiko
journal or publication title	IEEE Transactions on Plasma Science
volume	35
number	2-I
page range	197-203
year	2007-04-01
URL	http://hdl.handle.net/2297/6751

doi: 10.1109/TPS.2007.892709

Control of Nitrogen Atomic Density and Enthalpy Flow Into Reaction Chamber in Ar/N_2 Pulse-Modulated Induction Thermal Plasmas

Yasunori Tanaka, Takafumi Muroya, Kouhei Hayashi, and Yoshihiko Uesugi

(Invited Paper)

***Abstract*—Simultaneous control of the nitrogen atomic density and the enthalpy flow onto the specimen installed downstream of the plasma torch was accomplished using Ar/N_2 pulse-modulated induction thermal plasmas (PMITPs). Such simultaneous control was difficult to realize because the increasing input power into conventional nonmodulation thermal plasmas increases the number density of the nitrogen atoms, but it also increases the enthalpy flow onto the specimen. The behavior of the excited nitrogen atoms was measured through spectroscopic observation. The specimen's surface temperature was measured using a radiation thermometer. Then, the net enthalpy flow onto the specimen was estimated. Results showed that the modulation of coil current increases the time-averaged nitrogen atomic density and decreases the time-averaged enthalpy flow during the modulation cycle onto the specimen irradiated by the Ar/N_2 PMITP. This result was confirmed by results from the developed 2-D two-temperature chemical nonequilibrium model of the Ar/N_2 PMITP.**

***Index Terms*—Enthalpy flow, nitrogen atomic density, pulse-modulated induction thermal plasma (PMITP).**

I. Introduction

INDUCTIVELY coupled thermal plasmas have been widely used for material processing such as syntheses of diamond films, fullerenes, nanopowders, thermal-barrier coatings, etc. [1]–[9]. Its wide use is attributable to some advantages offered by inductively coupled thermal plasma: high temperature; high radical density; and little contamination. However, it has been pointed out that thermal plasma has a very high heavy-particle temperature, which can cause thermal damage to substrates and grown films. For that reason, a simple method for control of the thermal plasma's temperature is necessary.

To control this high enthalpy or high heavy-particle temperature of the thermal plasma, we developed a pulse modulated induction thermal plasma (PMITP) system [10]–[13]. This system can modulate the amplitude of the coil current sustaining thermal plasmas. The modulated thermal plasma enables control of the temperature, chemical-reaction, and gas-flow fields in thermal plasmas in the time domain. We have investigated dynamic behaviors of PMITP fundamentally through experimental and numerical approaches [14]–[19]. The investigations described above revealed that the coil-current modulation imparts great temperature and density disturbances in thermal plasmas. Furthermore, it enables the control of thermal plasma temperature in the time domain [19]. Moreover, it can promote chemical and thermal nonequilibrium states, even in high-power atmospheric-pressure plasmas.

Such a PMITP has been used for some material processing. For example, Ohashi *et al.* recently applied a PMITP to hydrogen doping on ZnO [20], [21]. Results of that study showed that irradiation of the $Ar\text{-}H_2$ PMITP can dope hydrogen atoms into ZnO and improve its photoluminescence. However, few reports have addressed applications of the PMITP to other material processes. We are now trying to apply a PMITP to surface nitriding of metals.

This paper describes experimental results of simultaneous control of the density of nitrogen atoms and the estimated enthalpy flow [22]. Spectroscopic observation was carried out to measure the radiation intensity of the nitrogen atomic line for different modulation conditions for the PMITP. The titanium specimen was installed downstream of the plasma torch; its surface temperature was measured using a radiation thermometer. Experimental results reveal that modulation of the coil current causes both an increase in the time-averaged nitrogen atomic density and a decrease in the time-averaged enthalpy flow onto the specimen surface during the modulation cycle. Such simultaneous control has been difficult using only conventional steady-state-induction thermal plasmas. Furthermore, numerical simulation of Ar/N_2 PMITP was made using our recently developed 2-D two-temperature chemically nonequilibrium model [19]. The simulation result supports the experimental results of the simultaneous control of nitrogen atom and enthalpy flow.

II. Parameters in Pulse Modulation of the Coil Current

Fig. 1 depicts the schematic waveforms of a typical pulse-amplitude-modulated coil current for sustaining the PMITP.

Manuscript received September 28, 2006; revised January 22, 2007.

Y. Tanaka, T. Muroya, and K. Hayashi are with the Division of Electrical Engineering and Computer Science, Kanazawa University, Kakuma, Kanazawa 920-1192, Japan (e-mail: tanaka@ec.t.kanazawa-u.ac.jp).

Y. Uesugi is with the Graduate School of Natural Science, Kanazawa University, Kakuma, Kanazawa 920-1192, Japan.

Color versions of one or more of the figures in this paper are available online at http://ieeexplore.ieee.org.

Digital Object Identifier 10.1109/TPS.2007.892709

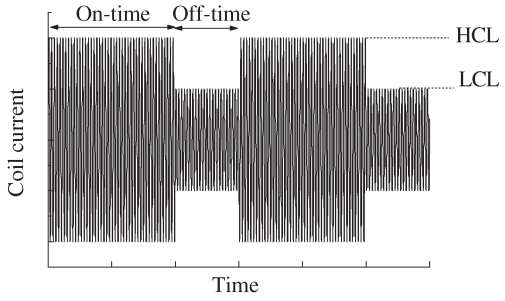

Fig. 1. Definition of parameters in the pulse-modulation operation.

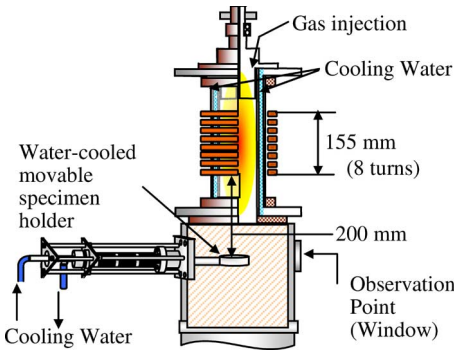

Fig. 2. Configuration of the plasma torch and the specimen holder.

The coil current has a fundamental frequency of 450 kHz in this paper. The amplitude of the coil current is modulated with a modulation cycle on the order of milliseconds. For the coil-current-modulation case, we define the following four additional control parameters: "higher current level (HCL)," "lower current level (LCL)," "on-time (time period with the HCL)," and "off-time (time period with the LCL)." These parameters are also indicated in Fig. 1. These parameters can be set independently from one another to obtain different dynamic states of a PMITP [16]. Furthermore, we define the "shimmer current level (SCL)" as the ratio LCL/HCL. The condition SCL $= 100\%$ corresponds to the nonmodulation operation.

III. Experimental Setup and Experimental Conditions

A. Plasma Torch and Reaction Chamber

Fig. 2 shows a schematic diagram of the plasma torch and the reaction chamber for PMITPs. The plasma torch comprises two coaxial quartz tubes with 330-mm length. The inner tube has a 70-mm inner diameter. Between these two coaxial tubes, cooling water is allowed to flow to maintain the tube wall temperature at 300 K. This plasma torch has an eight-turn induction coil around the quartz tube. Downstream of this plasma torch, a water-cooled reaction chamber is installed. In the reaction chamber, a water-cooled specimen holder was installed. This specimen holder held a 15-mm-diameter 5-mm-thick titanium specimen. The specimen was irradiated directly by an Ar/N_2 PMITP for its surface-nitriding processing. The Ar/N_2 gas mixture was supplied as a sheath gas with a swirl along the interior of the inner quartz tube from the top of the plasma torch. The total gas flow rate was fixed at 100.0 slpm $(=$ l/min$)$. The nitrogen gas flow rate Q_{N_2} was set to a value of

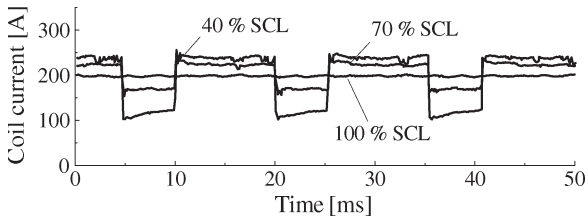

Fig. 3. Coil-current amplitude for fixed-power operation.

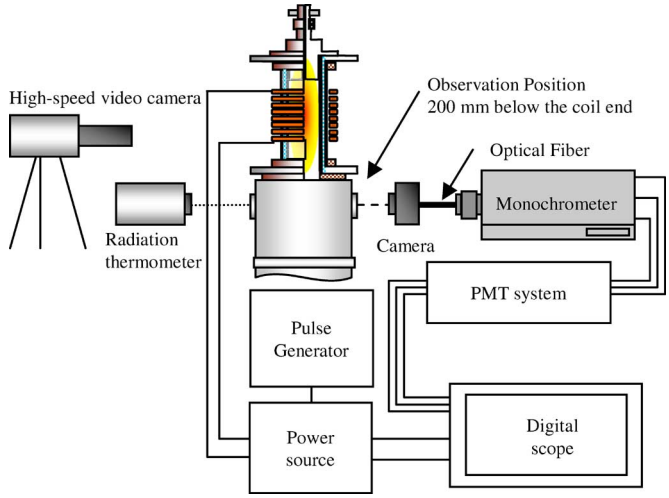

Fig. 4. Measurement systems.

2.0 or 4.0 slpm. For stable operation of the PMITP, the nitrogen gas flow rate is limited to 5.0 slpm in this experiment because too much addition of nitrogen gas will cause the PMITP to be extinguished. Pressure inside the chamber was fixed to 30 kPa (230 torr) using an automatic-feedback pressure controller.

The modulated coil current was supplied with a metal-oxide-semiconductor field-effect-transistor (MOSFET) inverter power supply to the induction coil. The "on-time" and "off-time" were set, respectively, to 10 and 5 ms in this experiment. In this paper, we fixed the time-averaged input power to the MOSFET inverter power supply at the same value of 15 kW for any SCL condition. This fixed power control can be realized using a higher HCL and a lower LCL to the current amplitude in the nonmodulation condition, as indicated in Fig. 3.

B. Measurement Systems

Fig. 4 depicts the measurement systems. Spectroscopic observations were carried out to measure the time evolution in the radiation intensities of the nitrogen atomic line at 746.8 nm and of the continuum at 756 nm. By subtracting the continuum from the radiation intensity at 746.8 nm, the net radiation intensity of the nitrogen atomic line is obtainable. The observation position was set to a position at 200 mm below the coil end, which corresponds to the inlet of the reaction chamber installed downstream of the plasma torch. This measurement shows the behavior of the nitrogen atoms excited at a level $2p^2(^3P)3p$ with 96 750 cm^{-1} in the observation region [23], because the measured radiation intensity is proportional to the number of the excited nitrogen atoms. Simultaneously, the surface temperature of the titanium specimen was measured

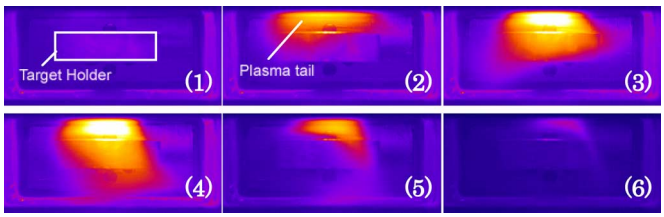

Fig. 5. Dynamic behavior of the plasma tail. The gas flow rate of Ar/N_2 is 98/2 slpm.

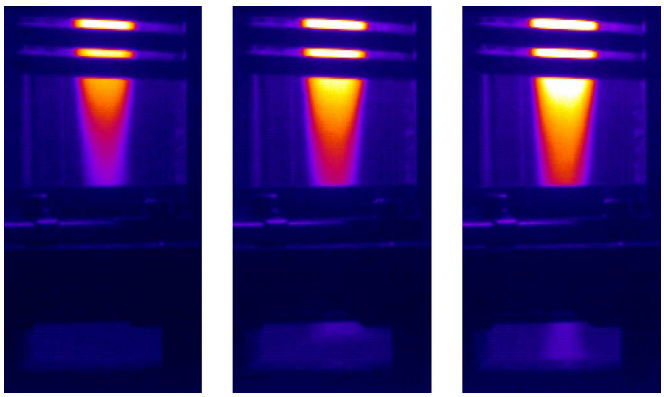

Fig. 6. Images of the Ar/N_2 PMITPs. Left: SCL SCL $= 100\%$. Center: SCL $= 70\%$. Right: SCL $= 40\%$. The gas flow rate of Ar/N_2 is 98/2 slpm.

using a radiation thermometer. The coil current was measured using a high-frequency current transformer. A high-speed video camera with a complementary metal–oxide semiconductor (CMOS) optical array was used to capture the dynamic behavior of the PMITP. The CMOS optical array has sensitivity for visible light between 400–800 nm. The exposure time was set to 10 μs, and the frame rate was fixed at 3200 frames/s.

IV. Results and Discussion

A. Dynamic Behavior of a PMITP Recorded by a High-Speed Video Camera

Fig. 5 shows the dynamic behavior of the tail part of the Ar/N_2 PMITP as recorded using the high-speed video camera. The respective gas flow rates of Ar and N_2 are 98 and 2 slpm, and the SCL is 40%. The time increment of the images in Fig. 5 is 1.0 ms. In panel (2), the plasma tail is visible, extending from the upper side according to "on-time" operation. This plasma tail extends to the specimen holder with rotation motion in panels (2)–(5). This rotation motion originates from a supplied swirl gas. The plasma tail goes to the upper side again in panels (5)–(6) in "off-time." These motions are repeated periodically according to coil-current modulation.

Fig. 6 indicates images of the Ar/N_2 PMITP for SCL $= 100\%$, 70%, and 40%. These images are taken when the visible-light-emission area from each PMITP is maximum. It is apparent that the visible-light-emission area from the PMITP for SCL $= 40\%$ is greater than those for SCL $= 100\%$ and 70%. This is true because a lower SCL case has a higher HCL in the fixed-input-power operation, as described in the previous section. Consequently, a longer plasma tail is realized in the lower SCL case. These longer plasma tails are inferred to promote surface-nitriding processing of the titanium specimen.

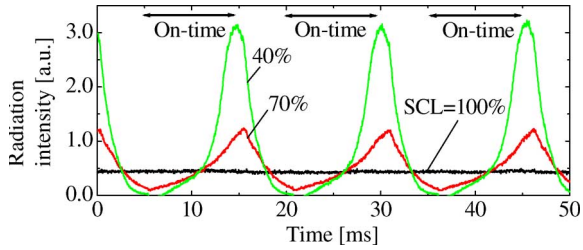

Fig. 7. Time evolutions in the radiation intensity of the nitrogen atomic line at 746 nm emitted from Ar/N_2 PMITP. The gas flow rate of Ar/N_2 is 96/4 slpm. Spectroscopic observation position was on the center axis of the plasma torch at 200 mm below the coil end.

B. Effects of Coil-Current Modulation on the Radiation Intensity of Nitrogen Atomic Line

For surface-nitrodiation processing using thermal plasmas, the neutral nitrogen atomic density is an extremely important factor. The radiation intensity of nitrogen atomic line at 746.8 nm was measured to estimate the behavior of the nitrogen atomic density. The measured radiation intensity is proportional to the number of the excited nitrogen atoms as described previously, which indicates an index of nitrogen excited atomic density. Fig. 7 shows the time evolution in the radiation intensity of the nitrogen atomic line from the Ar/N_2 PMITP for SCL of 100%, 70%, and 40%. The nitrogen gas flow rate Q_{N_2} is 4.0 slpm. It is apparent that the measured radiation intensity is also modulated according to the coil-current modulation. For modulation cases, i.e., for SCL $= 70\%$ and 40% cases, periodic peaks exist in the time evolution in the radiation intensity. The magnitudes of these peaks increase with reduction of SCL. This result demonstrates that the pulse modulation of the coil current increases the instantaneous density of the excited nitrogen atom in the observation region, i.e., at the inlet of the reaction chamber.

For surface-nitriding processing, the time-averaged density and the instantaneous value are important because some nitriding processes require a longer time than the pulse-modulation cycle. Consequently, the time-averaged radiation intensity was evaluated using the following equation:

$$I_{\mathrm{N746}}^{\mathrm{ave}} = \frac{1}{T_{\mathrm{cyc}}} \int_{t}^{t+T_{\mathrm{cyc}}} I_{\mathrm{N746}}(\tau)d\tau. \tag{1}$$

In that equation, $I_{\mathrm{N746}}^{\mathrm{ave}}$ denotes the time-averaged radiation intensity of the nitrogen atomic line, $I_{\mathrm{N746}}(\tau)$ represents the instantaneous radiation intensity of the nitrogen atomic line, T_{cyc} is the modulation cycle, and t, τ indicate the time. Fig. 8 shows the time-averaged radiation intensity of the nitrogen atomic line as a function of SCL for $Q_{N_2} = 4.0$ slpm. The time-averaged radiation intensity is normalized in reference to that at SCL $= 100\%$. The important point in Fig. 8 is that the time-averaged radiation intensity increases with decreasing SCL, meaning that the time-averaged nitrogen density as well as the

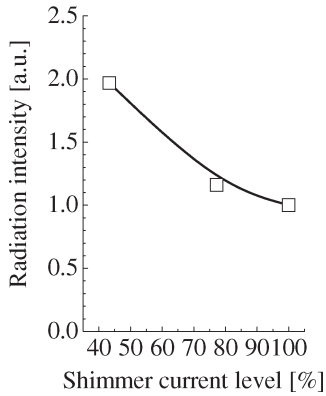

Fig. 8. Time-averaged radiation intensity of the nitrogen atomic line at 746 nm as a function of SCL. The gas flow rate of Ar/N_2 is 96/4 slpm. Spectroscopic observation position was on the center axis of the plasma torch at 200 mm below the coil end.

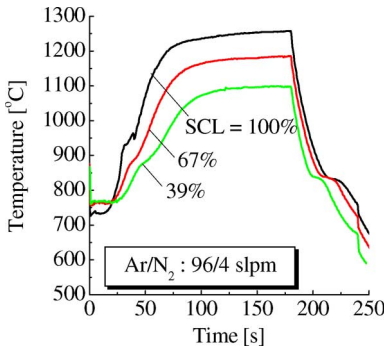

Fig. 9. Time variation in the surface temperature of titanium specimens irradiated by the Ar/N_2 PMITP. The gas flow rate of Ar/N_2 is 96/4 slpm.

instantaneous value increase because of the modulation of the coil current.

C. Effects of Coil-Current Modulation on the Specimen Surface Temperature

We also measured the specimen's surface temperature to elucidate effects of coil-current modulation on the enthalpy flow of the PMITP. The surface temperature is also an important factor for nitriding processing and for mitigating thermal damage. Fig. 9 depicts the time variation in the surface temperature of titanium specimens for different SCL cases. This surface temperature was measured with a radiation thermometer. The Ar/N_2 PMITP was irradiated from $t = 0$ s in this figure. After irradiation of the Ar/N_2 PMITP, the surface temperature increases with time. The surface temperature is almost saturated at about 100 s after irradiation. The irradiation of the Ar/N_2 PMITP was stopped at $t = 180$ s. After irradiation of the Ar/N_2 PMITP, the surface temperature decreases rapidly with time. It is noteworthy that the surface temperature variation depends on the SCL, although the input power to the inverter power supply is the same value of 15 kW for all cases.

In the estimation of the surface temperature, it is expected that the radiation from the plasma affects the determination of the surface temperature during the plasma irradiation. However, as shown in Fig. 9, there is no stepped change in the estimated surface-temperature curve just at plasma extinction,

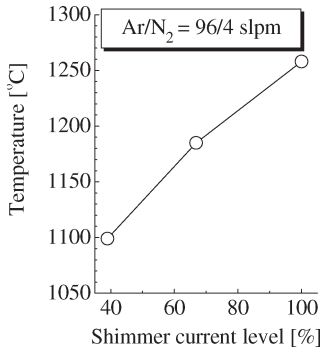

Fig. 10. Surface temperature of the titanium specimens irradiated by the Ar/N_2 PMITP as a function of SCL. The gas flow rate of Ar/N_2 is 96/4 slpm.

whereas the estimated surface temperature continuously and then gradually decreases with time from $t = 180$ s. Note that the vertical axis of this figure is in unit of seconds. Provided that plasma radiation affected the estimated temperature, it would change in step function form just after plasma extinction. From the above consideration, the plasma radiation does not so much affect the determination of the surface temperature if the surface temperature exceeds 750 K. However, when the surface temperature is lower than 750 K, which causes less thermal radiation from the surface, the plasma radiation affects the determination of the surface temperature. In addition, the emissivity influences the determination of the surface temperature. However, there is little data on the emissivity for a mixture of titanium–titanium nitride. Also, the emissivity is influenced by the roughness of the surface. In this estimation, we only used 0.6 as the emissivity of pure titanium. In spite of the above, the temperature plateau due to phase transition from Ti-β to Ti-α in Ti ingot inside the specimen can also be seen around $t = 200$ s at 850 °C for each of the curves in Fig. 9. The valid phase-transition temperature is 893 °C according to [24]. These values are close to one another. From the consideration, the error in the absolute value of the estimation temperature can be estimated about 50° in this case. The relative value of the surface temperature can be compared among these three curves in Fig. 9.

Fig. 10 indicates the surface temperature at $t = 180$ s after irradiation of the Ar-PMITP as a function of the SCL. This figure shows clearly that reducing the SCL decreases the surface temperature. The surface temperature is governed by the following equation:

$$\rho_s C_s \frac{\partial T_s}{\partial t} V_s = P_{\mathrm{net-in}} - \epsilon \sigma_b \left(T_s^4 - T_a^4\right) S_s \qquad (2)$$

where ρ_s and C_s, respectively, represent the mass density and the specific heat of the titanium specimen, V_s and S_s, respectively, denote the volume and surface area of the specimen, T_s is the surface temperature of the specimen, T_a is the ambient temperature, $P_{\mathrm{net-in}}$ is the net input power from heat transfer including cooling losses due to convection from a large disturbance in gas flow, ϵ is the emissivity of the surface material, and σ_b is the Stefan–Boltzmann constant. Quantity $P_{\mathrm{net-in}}$ was estimated through this equation and the time variation in the surface temperature in Fig. 9. Fig. 11 shows the $P_{\mathrm{net-in}}$ versus

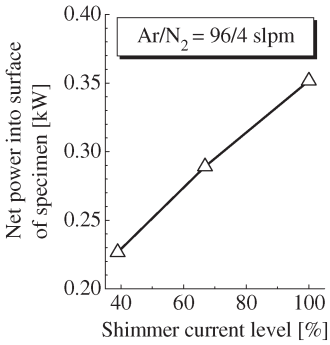

Fig. 11. Net power onto the surface of the titanium specimen irradiated by the Ar/N_2 PMITP. The gas flow rate of Ar/N_2 is 96/4 slpm.

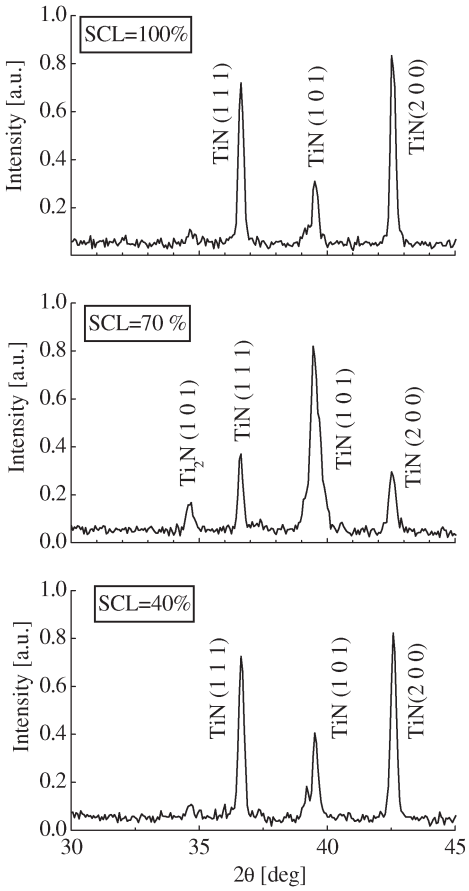

Fig. 12. Examples of XRD spectra for the specimen surface irradiated by the Ar/N_2 PMITP. The gas flow rate of Ar/N_2 is 98/2 slpm. The irradiation time is 5 min. The surface temperature of specimen is not controlled.

the SCL. For SCL $= 100\%$, $P_{\mathrm{net-in}}$ is 0.35 kW. This value is decreased by reduction of SCL.

Reducing SCL increases the excited nitrogen atomic density, as described in the previous section. Consequently, reducing SCL, i.e., the modulation of the coil current simultaneously causes both an increase in the excited nitrogen atomic density and a decrease in the $P_{\mathrm{net-in}}$.

D. X-Ray-Diffraction (XRD) Analysis of the Irradiated Specimen Surface

The specimen surface irradiated by an Ar/N_2 PMITP was analyzed by XRD to find the effect of the current modulation on the specimen surface composition. Fig. 12 shows examples of XRD spectra for the specimen surface irradiated by Ar/N_2 PMITP. The Ar and N_2 gas flow rates were 98 and 2 slpm, respectively. In this paper, we do not use hydrogen to simplify the experimental condition. The irradiation time is 5 min for all cases. As shown, XRD spectra for TiN (1 1 1), TiN (1 0 1), and TiN (2 0 0) can be seen in case of SCL $= 100\%$, i.e., nonmodulation case. On the other hand, at SCL $= 70\%$, the intensities of TiN (1 1 1) and TiN (2 0 0) decreases while those of TiN (1 0 1) increases and the spectrum of Ti_2N (1 0 1) appears. At further lower SCL, i.e., SCL $= 40\%$, the XRD spectra is again similar to that at SCL $= 100\%$, although the modulation condition (then the surface temperature) is different. As a result, the influence of the coil-current modulation is clearly apparent in XRD spectra for the irradiated surface even at the same input power and at the same specimen position. Although the details of structural-analyzing results should be investigated in the future work, it can be emphasized that the coil-current-modulation effects the surface structure. For surface nitriding of titanium, the surface temperature and nitrogen atomic density play an important role. These are both changed by the modulation coil current as described previously.

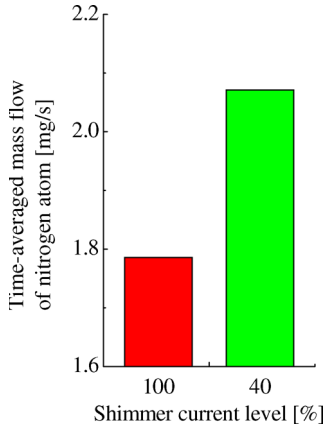

Fig. 13. Calculated time-averaged mass flow of nitrogen atom from the Ar/N_2 PMITP into the specimen position. The gas flow rate of Ar/N_2 is 96/4 slpm.

E. Numerical Simulation

We developed a 2-D two-temperature chemically nonequilibrium model of the Ar/N_2 PMITP [18], [19]. This model solves a set of mass-conservation equations of a bulk plasma, momentum-conservation equations, an energy-conservation equation for electrons, an energy-conservation equation for heavy particles, a mass-conservation equation of each species, and a Maxwell equation for the vector potential with a help of the equation of state and the equation of charge neutrality. Furthermore, in the present model, the swirl effect and demixing effect for each of species were also taken into account. From this numerical calculation result, we computed the time-averaged mass flow of nitrogen atom and the time-averaged enthalpy flow onto the specimen position for SCL $= 100\%$ and 40%.

Fig. 13 shows the calculated time-averaged mass flow of nitrogen atom from the Ar/N_2 PMITP into the specimen position

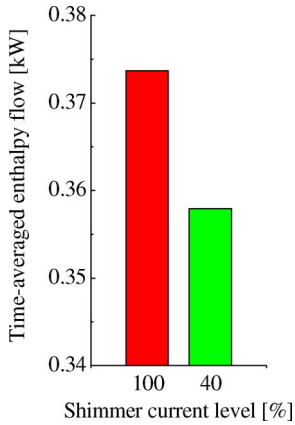

Fig. 14. Calculated time-averaged enthalpy flow from the Ar/N_2 PMITP into the specimen position. The gas flow rate of Ar/N_2 is 96/4 slpm.

by decreasing SCL. This quantity was calculated through the following equation:

$$M_{\mathrm{N}}^{\mathrm{ave}} = \frac{1}{T_{\mathrm{cyc}}} \int_{t}^{t+T_{\mathrm{cyc}}} M_{\mathrm{N}}(\tau) d\tau \tag{3}$$

$$M_{\mathrm{N}}(\tau) = 2\pi \int_{0}^{R} \rho Y_{\mathrm{N}} u r dr \Big|_{z=z_0} \tag{4}$$

where r and z, respectively, denote the radial and axial position, ρ is the mass density of the plasma, Y_{N} is the mass fraction of nitrogen atom, u is the axial gas-flow velocity, R is the radius of the specimen, and z_0 is the axial position of the specimen surface. As indicated in Fig. 13, $M_{\mathrm{N}}^{\mathrm{ave}}$ increases with decreasing SCL from 100% to 40%, meaning that the numerical simulation of Ar/N_2 PMITP also indicates an increase in the time-averaged mass flow of nitrogen atoms onto the specimen surface position. This increase in the time-averaged mass flow of the nitrogen atom arises from the chemically nonequilibrium condition, in which the nitrogen association needs milliseconds to reach its equilibrium condition.

On the other hand, Fig. 14 indicates the calculated time-averaged enthalpy flow from the Ar/N_2 PMITP into the specimen surface position. This quantity is calculated similarly using the following equation:

$$H^{\mathrm{ave}} = \frac{1}{T_{\mathrm{cyc}}} \int_{t}^{t+T_{\mathrm{cyc}}} H(\tau) d\tau \tag{5}$$

$$H(\tau) = 2\pi \int_{0}^{R} \rho h u r dr \Big|_{z=z_0} \tag{6}$$

where h is the enthalpy of the heavy particle. This Fig. 14 indicates that a reduction of the SCL from 100% to 40% decreases the H^{ave}.

In this way, the numerical simulation also supports the fact that the modulation of the coil current produces such an increase in the time-averaged mass flow of nitrogen atom and a decrease in the time-averaged enthalpy flow simultaneously, which is also obtained in the experiments as indicated in Figs. 8 and 11. However, these decreasing rates in the time-averaged mass and enthalpy flows by reduction of the SCL from the numerical simulation are lower than those obtained in the experiment in the previous section. It is inferred that reducing the SCL causes not only the reduction of the time-averaged enthalpy flow itself but also a large disturbance in the gas flow. This large disturbance in the gas flow may also increases cooling loss from the specimen due the thermal plasma.

V. Conclusion

Results of this paper demonstrated that an increased nitrogen atomic density and a decreased enthalpy flow onto the specimen installed downstream of the plasma torch simultaneously occurs using Ar/N_2 PMITP. An increase in the nitrogen atom density was made by spectroscopic observation, whereas the enthalpy flow onto the specimen was estimated using the measured surface temperature of the specimen. This simultaneous control of the time-averaged nitrogen atom density and the time-averaged enthalpy flow means that the PMITP can serve as a high-speed effective nitriding source with less thermal damage on the specimen. This result was also supported by our developed 2-D two-temperature chemically nonequilibrium model of the Ar/N_2 PMITP.

References

[1] J. O. Berghaus, J. L. Meunier, and F. Gitzhofer, "Monitoring and control of RF thermal plasma diamond deposition via substrate biasing," *Meas. Sci. Technol.*, vol. 15, no. 1, pp. 161–164, Jan. 2004.

[2] S. Matsumoto, M. Hino, and T. Kobayashi, "Synthesis of diamond films in an rf induction thermal plasma," *Appl. Phys. Lett.*, vol. 51, no. 10, pp. 737–739, Sep. 1987.

[3] C. Wang, A. Inazaki, T. Shirai, Y. Tanaka, T. Sakuta, H. Takikawa, and H. Matsuo, "Effect of ambient gas and pressure on fullerene synthesis in induction thermal plasma," *Thin Solid Films*, vol. 425, no. 1/2, pp. 41–48, Feb. 2003.

[4] B. Todorovic-Markovic, Z. Markovic, I. Mohai, Z. Karoly, L. Gal, K. Foglein, P. T. Szabo, and J. Szepvolgyi, "Efficient synthesis of fullerenes in RF thermal plasma reactor," *Chem. Phys. Lett.*, vol. 378, no. 3, pp. 434–439, Sep. 2003.

[5] S. L. Girshick, C. P. Chiu, R. Muno, C. Y. Wu, L. Yang, S. K. Singh, and P. H. McMurry, "Thermal plasma synthesis of ultrafine iron particles," *J. Aerosol Sci.*, vol. 24, no. 3, pp. 367–382, 1993.

[6] T. Ishigaki, S. M. Oh, J. G. Li, and D. W. Park, "Controlling the synthesis of TaC nanopowders by injecting liquid precursor into RF induction plasma," *Sci. Technol. Adv. Mater.*, vol. 6, no. 2, pp. 111–118, 2005.

[7] M. Shigeta, T. Watanabe, and H. Nishiyama, "Numerical investigation for nano-particle synthesis in an RF inductively coupled plasma," *Thin Solid Films*, vol. 457, no. 1, pp. 192–200, Jun. 2004.

[8] H. Huang, K. Eguchi, and T. Yoshida, "Novel structured yttria-stabilized zirconia coatings fabricated by hybrid thermal plasma spraying," *Sci. Technol. Adv. Mater.*, vol. 4, no. 6, pp. 617–622, Nov. 2003.

[9] W. R. Chen, X. Wu, B. R. Marple, and P. C. Patnaik, "Oxidation and crack nucleation/growth in an air-plasma-sprayed thermal barrier coating with NiCrAlY bond coat," *Surf. Coat. Technol.*, vol. 197, no. 1, pp. 109–115, Jul. 2005.

[10] T. Ishigaki, F. Xiaobao, T. Sakuta, T. Banjo, and Y. Shibuya, "Generation of pulse-modulated induction thermal plasma at atmospheric pressure," *Appl. Phys. Lett.*, vol. 71, no. 26, pp. 3787–3789, Dec. 1997.

[11] T. Sakuta, Y. Tanaka, Y. Hashimoto, and M. Katsuki, "Novel system of an inductively coupled thermal plasma with pulse amplitude modulation of electromagnetic field," *Electr. Eng. Jpn.*, vol. 138, no. 4, pp. 26–33, 2002.

[12] T. Sakuta, Y. Tanaka, K. C. Paul, M. M. Hossain, and T. Ishigaki, "Non-equilibrium effects in pulse modulated induction thermal plasma for advanced processing," *Trans. Mater. Res. Soc. Jpn.*, vol. 25, no. 1, pp. 35–38, 2000.

[13] Y. Tanaka and T. Sakuta, "Measurement of dynamic response time in pulse modulated thermal plasma," *Trans. Mater. Res. Soc. Jpn.*, vol. 25, no. 1, pp. 293–296, 2000.
[14] M. M. Hossain, Y. Tanaka, and T. Sakuta, "Transient nature of argon and molecular gas-seeded argon inductive thermal plasmas in pulse amplitude modulation approach," *Trans. Inst. Electr. Eng. Jpn.*, vol. 123-PE, no. 11, pp. 1333–1349, 2003.
[15] ——, "Dynamic responses of Ar-CO_2 and Ar-N_2 induction thermal plasmas in pulse modulation approach: A numerical analysis," *Thin Solid Films*, vol. 435, no. 1/2, pp. 19–26, Jul. 2003.
[16] Y. Tanaka and T. Sakuta, "Temperature control of Ar induction thermal plasma with diatomic molecular gases by pulse-amplitude modulation of coil-current," *Plasma Sources Sci. Technol.*, vol. 12, no. 1, pp. 69–77, 2003.
[17] ——, "Time-dependent two-dimensional chemical non-equilibrium modeling of Ar-N_2 pulse-modulated induction thermal plasma at atmospheric pressure for material processing," *Trans. Mater. Res. Soc. Jpn.*, vol. 29, no. 8, pp. 3403–3406, 2004.
[18] Y. Tanaka, "Two-temperature chemically non-equilibrium modelling of high-power Ar-N_2 inductively coupled plasma at atmospheric pressure," *J. Phys. D, Appl. Phys.*, vol. 37, no. 8, pp. 1190–1205, Apr. 2004.
[19] ——, "Time-dependent two-temperature chemically non-equilibrium modelling of high-power Ar-N_2 pulse-modulated inductively coupled plasmas at atmospheric pressure," *J. Phys. D, Appl. Phys.*, vol. 39, no. 2, pp. 307–319, Jan. 2006.
[20] N. Ohashi, T. Ishigaki, N. Okada, T. Sekiguchi, I. Sakaguchi, and H. Haneda, "Effect of hydrogen doping on ultraviolet emission spectra of various types of ZnO," *Appl. Phys. Lett.*, vol. 80, no. 16, pp. 2869–2871, Apr. 2002.
[21] N. Ohashi, T. Ishigaki, N. Okada, H. Taguchi, I. Sakaguchi, S. Hishita, T. Sekiguchi, and H. Haneda, "Passivation of active recombination centers in ZnO by hydrogen doping," *J. Appl. Phys.*, vol. 93, no. 10, pp. 6386–6392, May 2003.
[22] Y. Tanaka, T. Muroya, K. Hayashi, and Y. Uesugi, "Simultaneous control of numerical enhancement of N atom and decrease in heat flux into reaction chamber using Ar-N_2 pulse-modulated induction thermal plasmas," *Appl. Phys. Lett.*, vol. 89, no. 3, p. 031 501, Jul. 2006.
[23] *NIST Atomic Spectra Database ver. 3.10*, Gaithersburg, MD: Nat. Inst. Standards and Technol., Phys. Lab., Phys. Reference Data. [Online]. Available: http://physics.nist.gov/PhysRefData/ASD/index.html
[24] M. W. Chase, Jr. *et al.*, "JANAF thermochemical tables," 3rd ed., Suppl.1, *J. Phys. Chem. Ref. Data*, vol. 14, pp. 1818–1819, 1985.

Yasunori Tanaka was born in Japan in 1970. He received the B.S., M.S., and Ph.D. degrees in electrical engineering from Nagoya University, Nagoya, Japan, in 1993, 1995, and 1998, respectively.

In April 1998, he was appointed a Research Associate at Kanazawa University, Kanazawa, Japan, and where he has been working as an Associate Professor since August 2002 with the Graduate School of Natural Science. His research interests include arc-interruption phenomena and the fundamentals and applications of thermal plasmas by Magneto-Hydro-Dynamics (MHD) numerical simulation and experimental approaches. One of his papers was selected as one of the leading papers in *Journal of Physics D: Applied Physics* in 2004.

Dr. Tanaka is a member of IEE of Japan and the Japan Society of Plasma Science and Nuclear Fusion Research.

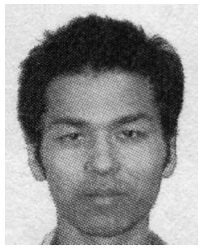

Takafumi Muroya was born in Japan in 1981. He received the B.S. and M.S. degrees in electrical engineering from Kanazawa University, Kanazawa, Japan, in 2004 and 2006, respectively.

He is currently with Kanazawa University, where he is engaged in RF thermal plasma applications.

Kouhei Hayashi was born in Japan in 1984. He received the B.S. degree in electrical engineering from Kanazawa University, Kanazawa, Japan, in 2005.

He is currently with Kanazawa University, where he is currently working for RF thermal plasma applications.

Yoshihiko Uesugi was born in Japan in 1955. He received the B.E., M.E., and D.E. degrees from Nagoya University, Nagoya, Japan, in 1977, 1979, and 1983, respectively.

After working as a Research Staff member of the Japan Atomic Energy Research Institute and an Associate Professor of Nagoya University, he is currently a Professor with the Graduate School of Natural Science at Kanazawa University, Kanazawa, Japan. His research interests are high-power plasma generation and application and magnetic-fusion experiments.

Dr. Uesugi is a member of IEE of Japan and the Japan Society of Plasma Science and Nuclear Fusion Research.